Hindawi
Advances in Materials Science and Engineering
Volume 2024, Article ID 9969064, 10 pages
https://doi.org/10.1155/2024/9969064

Research Article

Synthesis, Characterization, and Photocatalytic Activity of Cu-Doped MgO Nanoparticles on Degradation of Methyl Orange (MO)

Mebrihit Fissaha Gebreaneniya, Goitom Gebreyohannes Berhe, and Tesfamariam Teklu

Mekelle University, Department of Chemistry, Mekelle, Ethiopia

Correspondence should be addressed to Tesfamariam Teklu; betynatan@gmail.com

Received 3 November 2023; Revised 26 March 2024; Accepted 5 April 2024; Published 30 April 2024

Academic Editor: Michele Fedel

The purpose of this study is to synthesize Cu-doped MgO nanoparticles and test the performance of photocatalytic degradation of methyl orange (MO). $Mg(NO_3)_2$, $CuCl_2$, NaOH, and fresh *Calotropis procera* leaf extract were used as precursors. The prepared nanoparticles were characterized by using FT-IR, XRD, SEM, and UV-Vis spectrometer to study the functional group, crystal structure, surface morphology, and absorption edge, respectively. The wide band above 3000 cm^{-1} from the FT-IR spectrum corresponds to the stretching vibrations of flavonoids and phenolic compounds of *Calotropis procera* leaf extract. Furthermore, the Mg-O bonding of undoped MgO and Cu-doped MgO NPs is represented by new peaks which appeared at 831 and 835 cm^{-1}, respectively. The crystal size of undoped MgO and Cu-doped MgO nanoparticles is 13.04 nm and 12.08 nm, respectively. The SEM microstructure of pure MgO showed higher agglomeration than the Cu-doped MgO nanoparticles. The degradation efficiency of the Cu-doped MgO NPs was compared with that of the MgO NPs, and the photocatalytic activity of these NPs was evaluated using the photocatalytic degradation rates of MO dye. Cu-doped MgO NPs showed higher degradation efficiency than pure MgO NPs. The insertion of Cu in the MgO structure improved the photocatalytic efficiency of the MgO NPs under optimal conditions. Therefore, Cu-doped MgO exhibits high photocatalytic activity compared with undoped MgO nanoparticles under sunlight irradiation.

1. Introduction

The primary causes of the global contamination of water resources are growing urbanization and industrialization [1]. Water contamination is mostly caused by a considerable amount of synthetic colors among these pollutants. Remaining dye pollutants are primarily found in the wastewater from the paper, pulp, and textile industries. These toxins are dark in color, chemically stable, and non-biodegradable. Furthermore, the chemical sector releases hazardous and dangerous substances into water bodies, including phenols, herbicides, and pesticides [2].

Most of the textile industries emit organic dyes (phenol red, methyl orange, methyl red, methyl blue, and methyl violet), acidic gases, toxic gases, and heavy metals (Cd, Hg, and Pb) as raw materials which cause serious pollution to land and water [3]. Organic dyes inhibit light penetration through water, slow down photosynthesis reactions, hinder sunlight penetration, lower photosynthesis activity, and cause oxygen deficit, all of which have an impact on water quality. Furthermore, certain chemical dyes like azo dyes can cause mutagenic and carcinogenic effects [4]. Synthetic dyes, which are used in large quantities in the textile industry, are chemically stable and harmful to the environment. Because of their stability, azo dyes, such as methyl orange, are commonly used in the textile, paper, and food industries [5]. That is why research has been intensified on the treatment and management of azo dyes in wastewater to reduce their negative effects.

In developed countries, organic dyes from water and soil can be treated with modern technology. Photocatalytic nanoparticles have received a lot of attention due to their

unique properties compared to bulk materials. Metal oxide nanoparticles such as ZnO, Cu2O, TiO2, and MgO are suitable for the photodegradation of organic dyes. The degradation of methylene blue and Congo red was tested with ZnO and MgO nanoparticles [5, 6], respectively, at the laboratory scale. MgO nanoparticles show enhanced catalytic activity due to large surface area and high chemical stability [7]. MgO, on the other hand, absorbs only ultraviolet electromagnetic radiation due to its high bandgap energy. As a result, its photocatalytic activity under solar radiation is low, as only 5% of solar energy that reaches the earth is ultraviolet (UV) [8].

To increase photocatalytic activity, doped metals have recently been added to established photocatalysts such magnesium oxide (MgO). Transition metal doping changes the energy band gap, creates charge traps for photogenerated carriers, improves photocatalytic effectiveness by suppressing charge carrier recombination, and reduces kinetics [9]. It is commonly recognized that adding transition metals results in smaller nanoparticles with higher specific surface area and inhibits particle development. By increasing the surface area and surface defects of metal oxides through doping with copper, zinc, and silver, one can shift the optical absorbance towards the visible range [10]. It may also alter the optical characteristics, reduce the band gap, move the absorption band to a longer wavelength, and change the morphology of the MgO nanostructure; copper is the element of choice for doping MgO nanoparticles [11, 12].

Metal oxide nanoparticles can be synthesized by condensation, evaporation, sol-gel, precipitation, co-precipitation, and green methods [13]. Among theme, green synthesis has recently been of great interest to produce metal oxide nanoparticles such as ZnO, MnO_2, MgO, and TiO_2 [14]. In green synthesis, metal nitrate acts as an oxidizing agent and phytochemicals present in plant extracts act as a reducing and stabilizing agents for the synthesis of nanoparticles. Currently, plant-based synthesis is considered as the best alternative due to its stability and higher nanoparticle production rate [15].

Calotropis procera is a plant that contains various phytochemicals such as flavonoids, terpenoids, and phenols. Various biomolecules with functional groups such as C=C (alkenyl), C=N (amide), -O-H (phenolic and alcohol), N-H (amine), C-H, and COO- (carboxylic group) are primarily responsible for the reduction and stabilization of nanoparticles [16].

Therefore, this study including synthesis and characterization aimed to test Cu-doped MgO nanoparticles using leaf extract of *Calotropis procera* and photocatalytic degradation of methyl orange (MO) under solar radiation.

2. Materials and Methods

2.1. Chemicals. All the chemicals such as magnesium nitrate (99%), copper chloride dihydrate (98%), sodium hydroxide (99%), methyl orange (99.9%), and dimethyl sulfoxide (99%), deionized water, and fresh leaf of *Calotropis procera* were employed without further purification and were of analytical grade.

2.2. Plant Extraction and Synthesis of the Photocatalysts

2.2.1. Preparation of Calotropis procera Leaf Extract. Fresh leaf of *Calotropis procera* (Figure 1) was collected from Adwa District (located at 14°15′N and 38°52′E, with an elevation range from 1500 to 2700 m (a.s.l.)), Tigray, Northern Ethiopia [17]. The collected leaf was washed thoroughly using tap water, followed by deionized water until the dust particles and other undesired substances were removed. Then, the leaf was dried in open air to remove the residual moisture and changed into powder using a grinder. The powder was sieved using 250 micrometer sieve. About 4 g of the plant powder was boiled in 100 mL of deionized water for 15 min at 80°C. The leaf extract was cooled and filtered through Whatman No. 41 filter paper and centrifuged at 1500 rpm for 5 min to remove biomaterial residue. Finally, the filtrate of plant extract was stored in a refrigerator for further experiments [17].

2.2.2. Synthesis of MgO NPs Using Calotropis procera Leaf Extract. To prepare MgO nanoparticles, 0.1 M of $Mg(NO_3)_2$ was dissolved in 100 mL deionized water. The solution was mixed with 10 mL of leaf extract. Then, 5 mL of 1 M NaOH solution was added drop wise while continuously stirred for 3 h at 60°C. Upon the addition of NaOH solution a sharp change in color from light yellow to deep yellow was observed which confirmed the formation of $Mg(OH)_2$ nanoparticles. The precipitate was then centrifuged at 3000 rpm for 15 min, washed using deionized water several times, and dried in an oven for 12 h at 80°C. At this point, the yellow color product (mixture of MgO and $Mg(OH)_2$) did not show higher crystallinity. Then, it was calcined at 500°C for 3 h to remove organic impurities and obtain higher crystallinity MgO nanostructures [18].

2.2.3. Synthesis of Cu-Doped MgO NPs Using Calotropis procera Leaf Extract. To prepare Cu-doped MgO nanoparticles, 0.1 M of $Mg(NO_3)_2$ and 0.01 M of $CuCl_2$ were dissolved in 100 mL of deionized water. About 10 mL of leaf extract was added drop wise into the mixture with continuous stirring. Then, 5 mL of 1 M NaOH was also added drop wise with continuous stirring for 3 h at 60°C. The precipitate was centrifuged at 3000 rpm for 15 min and washed with deionized water several times to remove the impurities. After 12 h in an oven at 80°C, the precipitate changed into a dry powder. In addition, it was calcined at 500°C for 3 h in a muffle furnace [19].

2.3. Characterization. The crystal structures and average crystallite size of the samples were scanned using X-ray diffraction (XRD-7000, Shimadzu, Japan) equipped with a Cu-Kα radiation ($\lambda = 1.5406$ Å). The step scan mode is used to know crystal structures and average crystallite size in the range of 10° to 80°. A scanning electron microscope [20] (JSM-5610, JEOL, Japan) was used to examine the sample's surface morphology. The chemical functionality of the samples was analyzed using Fourier transform infrared

Figure 1: Image of *Calotropis procera* leaf.

spectroscopy (FT-IR, PerkinElmer, USA) in the range 4000-400 cm^{-1}. The optical properties of the nanoparticles were investigated using a PerkinElmer Lambda 35 spectrometer with a wavelength range of 200-800 nm [11].

2.4. Photocatalytic Degradation Studies. Methyl orange (MO) was selected as a model pollutant for photocatalysis due to excessive presence in textile effluents. Photocatalytic experiments were carried out in 500 mL beakers. The mixture of 1 g/L of MgO, Cu-doped MgO, and 200 mL of 10 ppm MO dye was stirred in a dark for 30 min to allow adsorption/desorption equilibrium before irradiating the sunlight [11]. The irradiation was then conducted under sunlight on sunny days to minimize fluctuations in solar intensity. After 20 min of irradiation, 10 mL of the heterogeneous mixture was withdrawn, centrifuged for 5 min at 3000 rpm, and then filtered through filter paper. The concentration of MO was determined by measuring the absorption intensity at maximum absorbance wavelength. The percentage degradation of MO solution was calculated using the following formula [21]:

$$\%\ \text{degradation} = \frac{A_0 - A_t}{A_0} \times 100, \quad (1)$$

where A_0 and A_t represent absorbance of MO at initial and each time interval, respectively.

3. Results and Discussion

3.1. Fourier Transform Infrared (FT-IR) Spectroscopy. The FT-IR spectra of *Calotropis procera* leaf extract, undoped MgO NPs, and Cu-doped MgO NPs are shown in Figure 2. The broad bands appeared around 3260-3300 cm^{-1} which correspond to N-H and O-H stretching vibrations from amino and phenolic compounds of flavonoids introduced from the *Calotropis procera* leaf extract. Minor peaks located at 2922 and 2852 cm^{-1} were attributed to C-H stretching

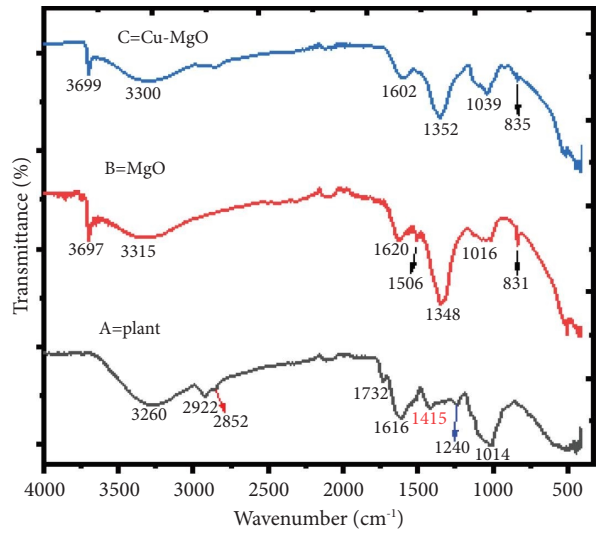

Figure 2: FT-IR spectra of (A) *Calotropis procera* leaf extract, (B) undoped MgO NPs, and (C) Cu-doped MgO NPs before calcinations.

vibrations of $-CH_3$ and $-CH_2$ aliphatic groups. The weak absorption peak at 1732 cm^{-1} is due to C=O stretching vibration of flavonoids. The strong peak at 1616 cm^{-1} represents the stretching vibration of aromatic C=C bond. Other scholar also reported occurrence of a broad absorption band at 3247 cm^{-1} from the investigation of *Calotropis gigantea* leaf extract which is peculiar characteristics of N-H and O-H starching vibration of amino and phenolic compounds of glycosides and flavonoids [22].

New peaks appeared at 831 cm^{-1} and 835 cm^{-1} which represent the stretching vibration of Mg-O bonding from MgO and Cu-doped Mg-O compounds, respectively. Cu-doped MgO showed slight shift to higher wave number which might be due to the introduction of Cu as a dopant. Other scholars also reported similar findings [23]. On the other hand, bands appearing at 3697 and 3699 cm^{-1} belong

to antisymmetric stretching vibration of $Mg(OH)_2$ crystal structure. These findings are in good agreement with the reported literature values [24].

3.2. XRD Analysis. The XRD diffractograms of undoped MgO and Cu-doped MgO NPs calcined at 500°C are shown in Figure 3. The XRD pattern of undoped MgO NPs appeared at $2\theta = 36.89°$, 42.88°, 62.24°, 74.59°, and 78.54° which correspond to (111), (200), (220), (311), and (222) plane of reflection, respectively. The diffraction peaks were well indexed to cubic crystal structure (JCPDS card No. 00-045-0946) with space group of Fm-3m. The sharp, clear line broadening of the diffraction peaks situated at 2θ showed that the as-synthesized MgO NPs have crystalline nature. This might be an indication of formation of pure phase of MgO NPs. These results are congruent with reported literature values [25]. The diffraction peaks of Cu-doped MgO at 2θ value of 36.86°, 42.87°, 62.22°, 74.59°, and 78.51° correspond to the Miller index of (111), (200), (220), (311), and (222). This shows that the XRD pattern of Cu-doped MgO changes towards the lower angle after doping with copper. These diffraction patterns of Cu-doped MgO nanoparticles are similar to the undoped MgO nanoparticles except for minor differences probably caused by the presence of trace impurities [21]. Moreover, smaller differences in ionic radii between Cu^{2+} (0.073 nm) and Mg^{2+} (0.066 nm) impacted the crystal lattice very little. This further enhanced creating the surface defects which might improve photocatalytic activity of MgO NPs [26].

The intensity of the strongest diffraction peak ($2\theta = 42.88°$) decreased and the full width at half maximum (FWHM) increased when Cu is doped. From the Debye–Scherrer equation (equation (2)), the intense peak was used to calculate the average crystallite size of the nanoparticles [31].

$$D = \frac{K\lambda}{\beta \cos\theta}, \tag{2}$$

where D is the crystallite size, λ is the wavelength of X-ray source (Cu-Kα radiation = 1.5406 Å), K is the shape factor = 0.94, θ is the Bragg angle, and β is the full width at half maximum in radian.

The crystallite domain sizes of all undoped MgO and Cu-doped MgO were found to be 12.56 nm, 13.04 nm, 13.06 nm, 13.97 nm, and 13.7 nm and 13.035 nm, 12.08 nm, 11.5 nm, 12.65 nm, and 12.28 nm, respectively. The crystallite size decreased in Cu-doped MgO compared to the pure MgO which might be due to the insertion of copper into MgO crystal lattice. The insertion of copper into the MgO nanoparticles lattices can disrupt the particle growth process, which could explain the reduction in crystallite size in Cu-doped MgO nanoparticles [21].

3.3. Surface Morphology Analysis. Surface morphology of the undoped MgO and Cu-doped MgO nanoparticles was examined by SEM as shown in Figure 4. SEM microstructure shows that surface morphology of MgO nanoparticles changes significantly after doping with copper. Pure MgO nanoparticles (Figure 4(a)) are connected to each other to make large network systems which have irregular pore sizes,

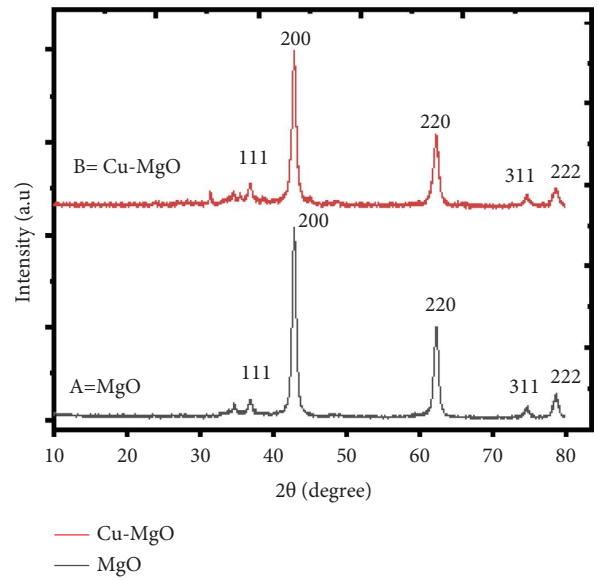

Figure 3: X-ray diffractograms of (A) undoped MgO and (B) Cu-doped MgO NPs calcined at 500°C.

shapes, and many agglomerations. The SEM micrographs of Cu-doped MgO nanoparticles (Figure 4(b)) indicate that the morphology is relatively uniformly distributed of spherical particles and exhibit good crystalline quality where agglomerations of particles are comparably less than the undoped MgO nanoparticles. This might be due to the copper doping which reduces the crystalline size of the particle which is similar to the reported value [27, 28]. This result is in line with the findings of crystallite size estimated from XRD measurements (Table 1).

3.4. Optical Property Analysis. UV-Vis diffuse reflectance spectroscopy was used to investigate the produced nanoparticles' electromagnetic radiation absorption region. The spectra for the absorption of light by MgO and Cu-doped MgO are given in Figure 5. MgO and Cu-doped MgO absorb at 336 nm and 400 nm, respectively. MgO absorption edge was in the UV region. Because of the copper, the Cu-doped MgO nanoparticle absorbed light in the visible region [29]. The absorption edges were increased to 400 nm by doping copper with MgO.

The band gap energy of nanoparticles is estimated by extrapolating the linear section of the graph between the modified Kubelka–Munk function $[F(R)h\nu]^2$ and photon energy ($h\nu$) [30] as shown in Figure 5(b). MgO band gap energy (3.7 eV) is reduced to 3.1 eV when it is doped with Cu. This clearly shows that the inclusion of Cu atoms contributes to the narrowing of MgO band gap, extending its absorption edge to the visible range and capturing more photons from sunlight [31, 35].

3.5. Effect of Photocatalytic Parameters on Degradation of Methyl Orange

3.5.1. Effect of Catalyst Loading. The photocatalytic degradation of methyl orange using the undoped MgO and Cu-doped MgO NPs under sunlight irradiation is shown in

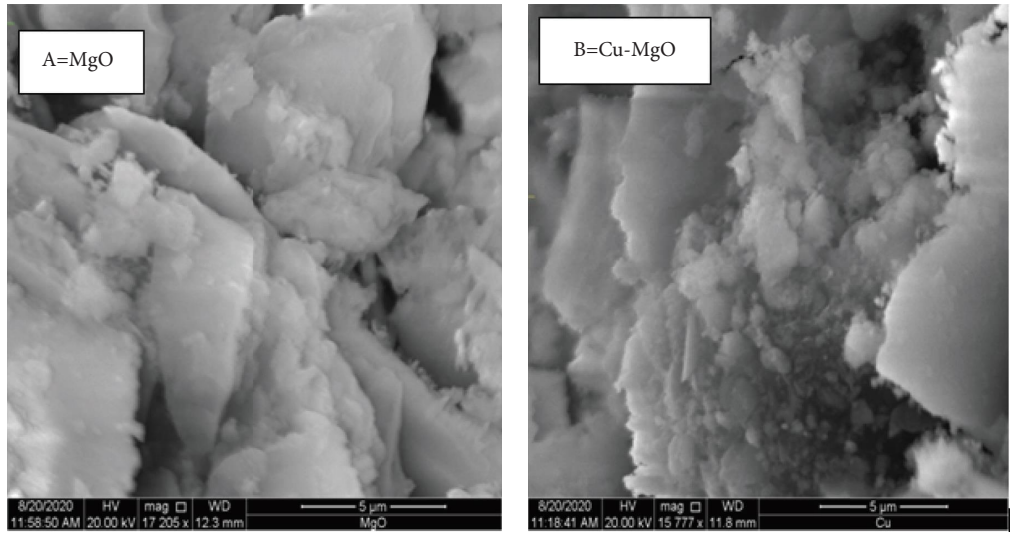

(a) (b)

Figure 4: SEM micrograph of (a) undoped MgO and (b) Cu-doped MgO NPs calcined at 500°C.

Table 1: Major crystalline size of as-synthesized nanoparticles.

Nanoparticles	2θ (deg)	FWHM (rad.)	Crystalline size (nm)	d-spacing
Undoped MgO	42.8756	0.65490	13.04	2.10758
Cu-doped MgO	42.8672	0.70710	12.08	2.10797

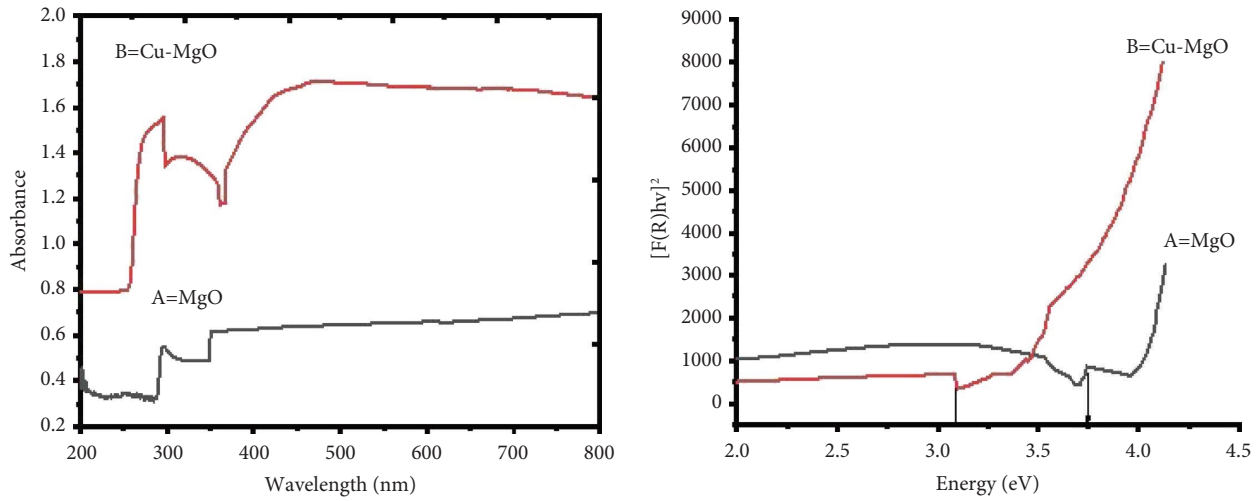

(a) (b)

Figure 5: (a) UV-Vis diffuse reflectance and (b) Kubelka–Munk function versus energy plots of undoped MgO and Cu-doped MgO NPs calcined at 500°C.

Figure 6. In order to study the effect of catalyst loading, a series of photocatalytic degradation experiments were carried out by varying the amounts of catalyst loading from 0.1 to 2 g/L solution with 10 ppm MO and 3 h irradiation time as optimized by Ashebir et al. [32]. After 3 h, the percentage of MO degradation increased from 72% to 85% as the amount of undoped MgO NPs loading increased from 0.1 to 1 g/L (Figure 6(a)). This might be due to an increase in the amount of catalyst which increases the availability of active sites on the catalyst surface, which in turn increases the number of hydroxyl and superoxide radicals. Similar findings have already been reported by other scholars [33]. However, further increase in catalyst dosage from 1 g/L to 2 g/L reduced the degradation of MO from 85% to 68% after 3 h. This might be due to blockage of light penetration by the existence of excessive amount of photocatalyst. Moreover,

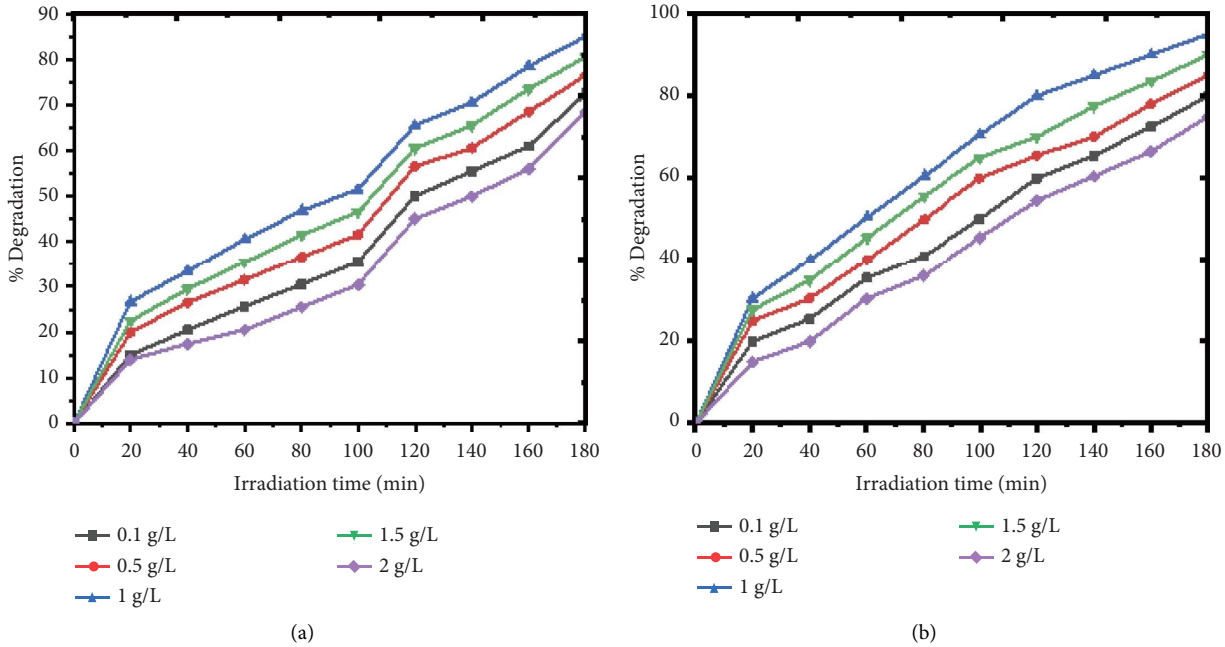

Figure 6: Effect of catalyst loading on the degradation of MO with (a) undoped MgO and (b) Cu-doped MgO NPs under irradiation.

agglomeration might also occur. When the catalyst concentration is higher, it reduces the surface area and decreases the degradation of the catalyst efficiency [34].

Similarly, when the amount of Cu-doped MgO nanoparticles increased from 0.1 g/L to 1 g/L, the percent of degradation also increased from 80% to 95% after 3 h (Figure 6(b)) [35]. This might be caused by an increase in catalyst loading, which would increase the photocatalyst surface area and reaction sites. However, as the catalyst dosage was increased beyond 1 g/L, the degradation efficiency further decreased. This could be due to the reduction of catalyst surface area [35]. Therefore, the degradation efficiency of Cu-doped MgO nanoparticles was higher than that of the undoped MgO nanoparticles. The optimum amount of the catalyst dosage was 1 g/L.

3.5.2. Effect of Concentration of Methyl Orange. The photocatalytic degradation experiment was carried out by varying the initial concentration of MO (10 to 17.5 mg/L) with an increment of 2.5 mg/L while catalyst loading and irradiation time were kept constant at 1 g/L and 3 h, respectively. As shown in Figure 7(a), by increasing the dye concentration from 10 mg/L to 17.5 mg/L, the degradation efficiency reduced from 88% to 60% after 3 h. The decrease in degradation efficiency with increasing dye concentration is due to a reduction in the amount of hydroxyl radicals, which in turn reduces the catalyst's degradation performance [36]. As indicated in Figure 7(b), when the initial concentration of MO increases from 10 mg/L to 17.5 mg/L, the percentage of degradation also decreased from 94% to 65% after 3 h and at 1 g/L of Cu-MgO nanoparticles. This might be due the existence of excess dye molecules with fixed amount of catalyst to compete for the active sites thus reducing the degradation rate. Moreover, high concentration of a dye also hinders light penetration [37].

The comparison of photocatalytic degradation efficiency of the undoped MgO and Cu-doped MgO nanoparticles for MO is shown in Figure 8. The photocatalytic degradation efficiency of the undoped MgO and Cu-doped MgO nanoparticles was compared in the degradation of MO using sunlight irradiation as source of energy. The degradation efficiency of the MO (10 ppm) after sunlight irradiation of aqueous solution using 1g/L undoped MgO and Cu-doped MgO photocatalyst were found to be 80% and 95%, respectively; after 3 h irradiation time. As a result of increased surface area from Cu-doping, the photocatalytic degradation efficiency was significantly increased. Despite the low MO concentration, it took about 180 minutes of irradiation to completely degrade MO in the presence of undoped MgO and Cu-doped MgO NPs. This is due to the photocatalyst being placed on a surface, which significantly reduces light absorption and dye interaction [28]. In general, the photocatalytic degradation efficiency of Cu-doped MgO nanoparticles is greater than that of undoped MgO nanoparticles. Even though there is no crystal size difference with the as-synthesized nanoparticles, Cu-doped has greater efficiency than undoped of MgO nanoparticles; this is possibly due to the narrow band gap energy [12].

The proposed degradation mechanism of MO by the undoped MgO and Cu-doped MgO photocatalytic nanoparticles is illustrated in Scheme 1. During the irradiation time, the undoped MgO photocatalysts could easily absorb the light energy to create holes (h_{VB}^{+}) in the valance band and electrons (e_{CB}^{-}) in the conduction band (equations (3) and (4)) [7]. Then, the holes and electrons can react with H_2O and oxygen already adsorbed at the surface of MgO nanoparticles to generate hydroxyl ($^{\cdot}OH$) and superoxide

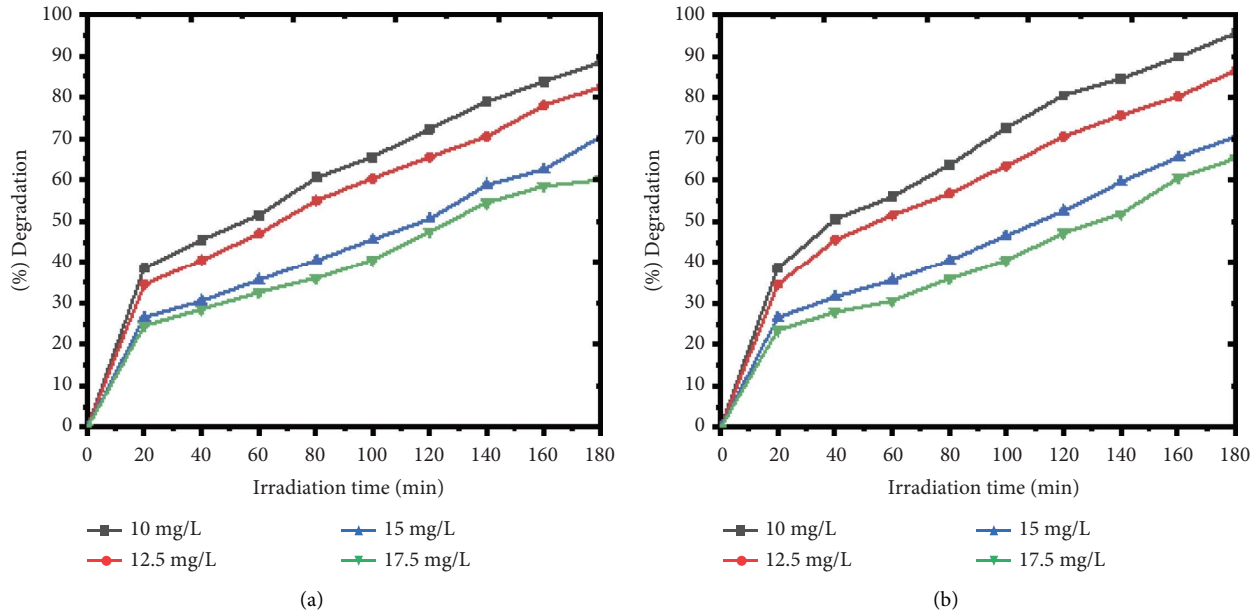

Figure 7: Effect of initial dye concentration on the photocatalytic degradation of MO under solar light using (a) undoped MgO and (b) Cu-doped MgO NPs.

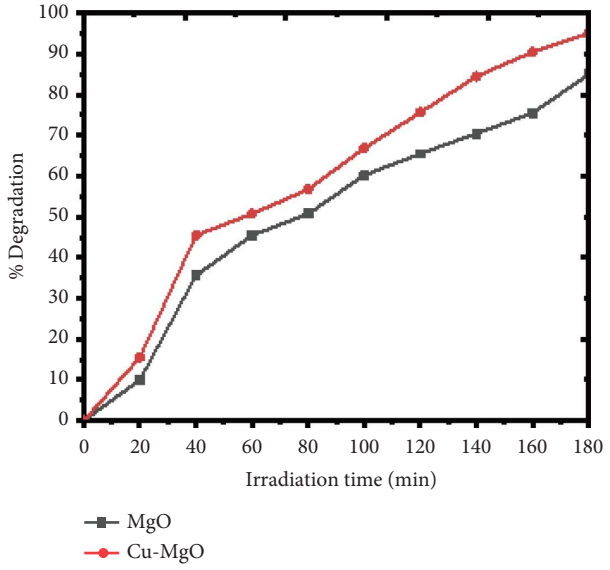

Figure 8: Photocatalytic efficiency comparison of undoped MgO and Cu-doped MgO NPs on the degradation of MO under solar light irradiation.

$$\mathrm{MgO} + h\nu \longrightarrow \mathrm{MgO}\left(h^{+}_{VB}\right) + \mathrm{MgO}\left(e^{-}_{CB}\right) \quad (3)$$

$$\mathrm{H_2O} \longrightarrow \mathrm{H^{+}} + \mathrm{OH^{-}} \quad (4)$$

$$\mathrm{MgO}\left(h^{+}_{VB}\right) + \mathrm{OH^{-}} \longrightarrow \mathrm{OH} \quad (5)$$

$$\mathrm{Cu^{2+}} + e^{-}_{CB} \longrightarrow \mathrm{Cu^{+1}}\,(\text{electron trap}) \quad (6)$$

$$\mathrm{Cu^{+1}} + \mathrm{O_2}\,(\text{ads}) \longrightarrow \mathrm{Cu^{2+}} + \mathrm{O_2^{-}}\,(\text{electron release}) \quad (7)$$

$$\mathrm{O_2^{-}} + \mathrm{H^{+}} \longrightarrow \mathrm{HO_2} \quad (8)$$

$$\mathrm{HO_2} + \mathrm{HO_2} \longrightarrow \mathrm{O_2} + \mathrm{H_2O_2} \quad (9)$$

$$\mathrm{H_2O_2} + \mathrm{O_2^{-}} \longrightarrow \mathrm{OH^{-}} + \mathrm{OH} + \mathrm{O_2} \quad (10)$$

$$\mathrm{OH} + \mathrm{Dye} \longrightarrow \mathrm{H_2O} + \mathrm{CO_2} \quad (11)$$

$$\mathrm{OH} + \mathrm{Dye} \longrightarrow \mathrm{H_2O} + \mathrm{CO_2} \quad (12)$$

(O_2^-) radicals (equations (5) and (6)). Copper is actually used to trap the photogenerated electron by acting as an electron sink to prevent the charge-carrier recombination. Furthermore, the Cu^{2+} ions trap electrons and convert into less stable Cu^{1+} ions which are ready to react with oxygen molecules used as oxidizing agent for superoxide formation (equations (7) and (8)). Finally, the hydroxyl ($^{\cdot}OH$) radicals and superoxide (O_2^-) radicals are readily available for further decomposition of MO (equation (9)) [12, 39]. The overall elementary reaction mechanisms are summarized from (3)–(12).

3.6. Kinetic Study of the Photocatalytic Degradation of MO. The rate of reaction for the photocatalytic degradation of MO using the undoped MgO and Cu-doped MgO NPs is shown in Figure 9. The graph of first-order kinetics was drawn by plotting $\ln(C_0/C_t)$ versus irradiation time. The experimental results demonstrated that photocatalytic degradation of MO is a first-order kinetic reaction. A good correlation coefficient ($R^2 > 0.97$) confirmed that the experimental data are nearly linearly fit [12, 40]. The photocatalytic degradation of MO using undoped MgO and Cu-doped MgO nanoparticles has rate constants of 0.00544 and

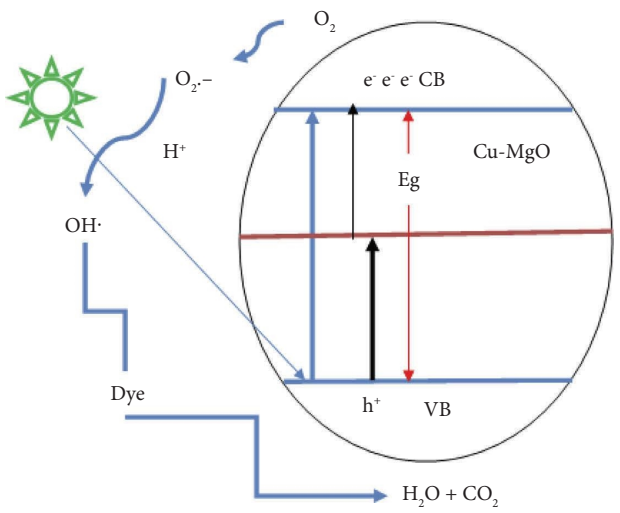

Scheme 1: Schematic representation of the photocatalytic degradation of MO using the undoped MgO NPs under sunlight irradiation [37].

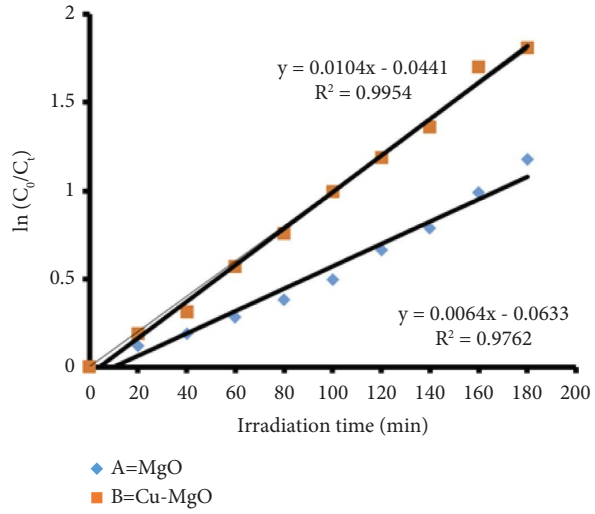

Figure 9: Graph of first-order kinetics for the photocatalytic degradation of MO using (A) undoped MgO and (B) Cu-doped MgO NPs.

0.0096 min^{-1}, respectively. The rate of kinetics for photocatalytic degradation of MO is more efficient for Cu-doped MgO nanoparticles.

4. Conclusion

Pure MgO and Cu-doped MgO nanoparticles were successfully synthesized by using *Calotropis procera* leaf extract as a natural reducing and stabilizer agent. The as-synthesized pure MgO and Cu-doped MgO NPs were characterized by FT-IR, XRD, SEM, and UV-Vis diffuse reflectance spectrophotometer. The FT-IR spectrum shows the presence of stretching vibrations of the O-H, N-H, and C= O groups involved in the stabilization of the nanoparticles. The XRD results confirmed that the inclusion of copper as a doping agent reduced the crystal size of the undoped MgO NPs. The SEM micrographs also revealed that the pure MgO NPs have irregular pore size and high agglomeration compared with the Cu-doped MgO NPs. The inclusion of Cu as a dopant for the MgO nanoparticles reduced the band gap energy from 3.7 to 3.1 eV. The as-synthesized Cu-doped MgO nanoparticles have better photocatalytic degradation efficiency than the undoped MgO nanoparticles for MO. The experimental results of as-synthesized nanoparticles for photocatalytic degradation of MO indicate that rate of degradation is dependent on initial dye concentration and catalyst loading. The kinetic reaction of MO for photocatalytic degradation was consistent first-order reaction.

As a result, Cu-doped MgO nanoparticles are considered an efficient solar light active photocatalyst for the removal of organic dyes from wastewater.

Data Availability

The data used to support the findings of this study are available from the first author upon request.

Conflicts of Interest

The authors declare that they have no conflicts of interest.

Acknowledgments

The first author acknowledges the financial support from Mekelle University (NORAD Project) (Grant ID: PG/MSc/CNCS/MU-NMBU/60/2020).

References

[1] T. Naseem and T. Durrani, "The role of some important metal oxide nanoparticles for wastewater and antibacterial applications: a review," *Environmental Chemistry and Ecotoxicology*, vol. 3, pp. 59–75, 2021.

[2] J. Kulkarni, R. Ravishankar, H. Nagabhushana et al., "Structural, optical and photocatalytic properties of MgO/CuO nanocomposite prepared by a solution combustion method," *Materials Today: Proceedings*, vol. 4, no. 11, pp. 11756–11763, 2017.

[3] C. R. Holkar, A. J. Jadhav, D. V. Pinjari, N. M. Mahamuni, A. B. Pandit, and A. B. Pandit, "A critical review on textile wastewater treatments: possible approaches," *Journal of Environmental Management*, vol. 182, pp. 351–366, 2016.

[4] Y. Liu, C. Li, J. Bao, X. Wang, W. Yu, and L. Shao, "Degradation of azo dyes with different functional groups in simulated wastewater by electrocoagulation," *Water*, vol. 14, no. 1, p. 123, 2022.

[5] T. S. Algarni, A. Abduh, A. Aouissi, and A. Al Kahtani, "Photodegradation of methyl orange under solar irradiation on Fe-doped ZnO nanoparticles synthesized using wild olive leaf extract," *Green Processing and Synthesis*, vol. 11, no. 1, pp. 895–906, 2022.

[6] N. T. Nguyen and V. A. Nguyen, "Synthesis, characterization, and photocatalytic activity of ZnO nanomaterials prepared by a green, nonchemical route," *Journal of Nanomaterials*, vol. 2020, pp. 1–8, 2020.

[7] R. Benisha, M. Amalanathan, M. S. M. Aravind et al., "Catharanthus roseus leaf extract mediated Ag-MgO

nanocatalyst for photocatalytic degradation of Congo red dye and their antibacterial activity," *Journal of Molecular Structure*, vol. 1262, 2022.

[8] J. Pachiyappan, N. Gnanansundaram, S. Sivamani, N. Sankari, N. Senthilnathan, and G. A. Kerga, "Preparation and characterization of magnesium oxide nanoparticles and its application for photocatalytic removal of rhodamine B and methylene blue dyes," *Journal of Nanomaterials*, vol. 2022, pp. 1–6, 2022.

[9] Z. M. Alaizeri, H. A. Alhadlaq, S. Aldawood et al., "Facile synthesis, characterization, photocatalytic activity, and cytotoxicity of Ag-doped MgO nanoparticles," *Nanomaterials*, vol. 11, no. 11, p. 2915, 2021.

[10] M. Ramezani Farani, M. Farsadrooh, I. Zare, A. Gholami, and O. Akhavan, "Green synthesis of magnesium oxide nanoparticles and nanocomposites for photocatalytic antimicrobial, antibiofilm and antifungal applications," *Catalysts*, vol. 13, no. 4, p. 642, 2023.

[11] Z. M. Alaizeri, H. A. Alhadlaq, S. Aldawood et al., "Facile synthesis, characterization, photocatalytic activity, and cytotoxicity of Ag-doped MgO nanoparticles," *Nanomaterials*, vol. 11, p. 2915, 2021.

[12] M. Shaheen, A. Bhatti, A. Ashar et al., "Synthesis of Cu-doped MgO and its enhanced photocatalytic activity for the solar-driven degradation of disperse red F_3BS with condition optimization," *Zeitschrift für Physikalische Chemie*, vol. 235, no. 11, pp. 1395–1412, 2021.

[13] B. A. Lemecho, F. K. Sabir, D. M. Andoshe et al., "Biogenic synthesis of Cu-doped ZnO photocatalyst for the removal of organic dye," *Bioinorganic Chemistry and Applications*, vol. 2022, Article ID 8081494, 10 pages, 2022.

[14] H. A. A. Jamjoum, K. Umar, R. Adnan, M. R. Razali, M. N. Mohamad Ibrahim, and M. N. Mohamad Ibrahim, "Synthesis, characterization, and photocatalytic activities of graphene oxide/metal oxides nanocomposites: a review," *Frontiers in Chemistry*, vol. 9, 2021.

[15] G. P, Krishna, P. Chandra et al., "Stephen Santhakumari, Photocatalytic activity induced by metal nanoparticles synthesized by sustainable approaches: a comprehensive review," *Frontiers in Chemistry*, vol. 10, 2022.

[16] T. R. Rahman, "Synthesis and characterization of MgO nanoparticles using neem leaves with their photocatalytic and antioxidant properties," *Saudi Journal of Medical Pharmaceutical Sciences*, vol. 7, pp. 348–357, 2021.

[17] V. V. Gawade, N. L. Gavade, H. M. Shinde, S. B. Babar, A. N. Kadam, and K. M. Garadkar, "Green synthesis of ZnO nanoparticles by using Calotropis procera leaves for the photodegradation of methyl orange," *Journal of Materials Science: Materials in Electronics*, vol. 28, no. 18, pp. 14033–14039, 2017.

[18] I. H. Shah, M. Ashraf, I. A. Sabir et al., "Green synthesis and Characterization of Copper oxide nanoparticles using Calotropis procera leaf extract and their different biological potentials," *Journal of Molecular Structure*, vol. 1259, 2022.

[19] A. Fatiqin, H. Amrulloh, and W. Simanjuntak, "Green synthesis of MgO nanoparticles using Moringa oleifera leaf aqueous extract for antibacterial activity," *Bulletin of the Chemical Society of Ethiopia*, vol. 35, no. 1, pp. 161–170, 2021.

[20] I. M, M. N. Khan, N. Akhtar et al., "Green synthesis of magnesium oxide nanoparticles using Dalbergia sissoo extract for photocatalytic activity and antibacterial efficacy," *Applied Nanoscience*, vol. 10, pp. 2351–2364, 2020.

[21] A. Gnanaprakasam, V. M. Sivakumar, and M Thirumarimurugan, "A study on Cu and Ag doped ZnO nanoparticles for the photocatalytic degradation of brilliant green dye. synthesis and characterization," *Water Science and Technology*, vol. 74, pp. 1426–1435, 2016.

[22] Y. S. Hii, J. Jeevanandam, and Y. S. Chan, "Plant mediated green synthesis and nanoencapsulation of MgO nanoparticle from Calotropis gigantea: Characterisation and kinetic release studies," *Inorganic and Nano-Metal Chemistry*, vol. 48, pp. 620–631, 2018.

[23] I. Gingaşu, D. C. Mîndru, L. Culiţă, G. Predoană, M. Petcu, and S. Petrescu Ciobanu, "MgO obtained by chemical and green synthesis methods and applied in photocatalytic degradation of methyl orange," *Revue Roumaine de Chimie*, vol. 66, pp. 463–473, 2021.

[24] L. Umaralikhan and M. J. M. Jaffar, "Green synthesis of MgO nanoparticles and it antibacterial activity," *Iranian Journal of Science and Technology, Transactions A: Science*, vol. 42, pp. 477–485, 2018.

[25] V. Rajendran, B. Deepa, and R. Mekala, "Studies on structural, morphological, optical and antibacterial activity of Pure and Cu-doped MgO nanoparticles synthesized by co-precipitation method," *Materials Today: Proceedings*, vol. 5, pp. 8796–8803, 2018.

[26] A. M, H. P. Kumar, S. C. Nagaswarupa et al., "UV-Sun light Photocatalytic and photoluminescence Studies of Rare-Earth-Doped (Sm^{3+}) MgO nano powders by Aloe Vera gel," *Materials Today: Proceedings*, vol. 4, pp. 11737–11746, 2017.

[27] R. M, Mohammad Shafiee, M. Kargar, and M. Ghashang, "Characterization and low-cost, green synthesis of Zn^{2+} doped MgO nanoparticles," *Green Processing and Synthesis*, vol. 7, pp. 248–254, 2018.

[28] I. A. Najem, S. J. Edrees, and F. Abd Rasin, "Structural and Magnetic Characterisations of Pb-Doped MgO Nanoparticles by a Modified Pechini Method," *IOP Conference Series: Materials Science and Engineering*, vol. 987, 2020.

[29] K. Ebrahimi, A. Hossienzadeh, R. Maleki, R. Ghanbari, M. Rezaee, and S. H. Puttaiah Safari, "Effects of doping zinc oxide nanoparticles with transition metals (Ag, Cu, Mn) on photocatalytic degradation of Direct Blue 15 dye under UV and visible light irradiation," *Journal of Environmental Health Science and Engineering*, vol. 17, pp. 479–492, 2019.

[30] M. R. Islam, M. Saiduzzaman, S. S. Nishat, A. Kabir, and S. F. U. Synthesis, "characterization and visible light-responsive photocatalysis properties of Ce doped CuO nanoparticles: a combined experimental and DFT+ U study," *Colloids and Surfaces A: Physicochemical and Engineering Aspects*, vol. 617, 2021.

[31] M. Adeel, I. Saeed, M. Khan, and N. Akram Muneer, "Synthesis and characterization of Co–ZnO and evaluation of its photocatalytic activity for photodegradation of methyl orange," *ACS Omega*, vol. 6, pp. 1426–1435, 2021.

[32] M. E. Ashebir, G. M. Tesfamariam, G. Y. Nigussie, and T. W. Gebreab, "Structural, optical, and photocatalytic activities of Ag-doped and Mn-doped ZnO nanoparticles," *Journal of Nanomaterials*, vol. 2018, 2018.

[33] A. M, B. Kumar, H. P. Mahendra, B. S. Nagaswarupa, C. R. Surendra, and K. Shetty Ravikumar, "Photocatalytic Studies of MgO Nano Powder; Synthesized by Green Mediated Route," *Materials Today: Proceedings*, vol. 5, 2018.

[34] S. R. Sowmya, G. M. Madhu, and M. Hashir, "Studies on Nano-Engineered TiO_2 Photo Catalyst for Effective Degradation of Dye," *IOP Conference Series: Materials Science and Engineering*, vol. 310, 2018.

[35] M. R. Al-Mamun, M. Z. I. Rokon, M. A. Rahim et al., "Enhanced photocatalytic activity of Cu and Ni-doped ZnO

nanostructures: A comparative study of methyl orange dye degradation in aqueous solution," *Heliyon*, vol. 9, 2023.

[36] T. L, L. T. Nguyen, A. T. Nguyen et al., "Preparation, characterization and photocatalytic activity of La-doped zinc oxide nanoparticles," *Materials*, vol. 12, p. 1195, 2019.

[37] A. Akram, Z. M. Fatima, Almohaimeed, and Q. Zafar, "Photocatalytic Degradation of Methyl Green Dye Mediated by Pure and Mn-Doped Zinc Oxide Nanoparticles under Solar Light Irradiation," *Adsorption Science & Technology*, vol. 2023, 2023.

[38] A. Ghaffar, M. Abbas, N. Naeem-ul-Hassan et al., "Hatem, Improved photocatalytic and antioxidant activity of olive fruit extract-mediated ZnO nanoparticles," *Antioxidants*, vol. 12, p. 1201, 2023.

[39] L. Pandian, R. Rajasekaran, and P. Govindan, "Synthesis, characterization and application of Cu doped ZnO nanocatalyst for photocatalytic ozonation of textile dye and study of its reusability," *Materials Research Express*, vol. 5, 2018.

[40] R. M, M. Islam, S. F. U. Rahman, S. F. U. Farhad, J. Podder, and J. Structural, "optical and photocatalysis properties of sol–gel deposited Al-doped ZnO thin films," *Surfaces and Interfaces*, vol. 16, pp. 120–126, 2019.